IPG 2025 7th International Pipeline Geotechnical Conference

IPG2025
6-7 November 2025, Bogota, Colombia

IPG2025-020

PROBABILISTIC APPROACHES TO ASSESSING CO-SEISMIC GEOHAZARD RISK FOR OIL AND GAS TRANSMISSION PIPELINES

Martin Zaleski
BGC Engineering Inc.
Vancouver, Canada

Adam Ballingall
BGC Engineering Inc.
Vancouver, Canada

Yolanda Alberto
BGC Engineering Inc.
Toronto, Canada

Daniela Welkner
BGC Engineering Inc.
Santiago, Chile

ABSTRACT

Pipelines are exposed to a range of seismic and co-seismic threats in seismically active regions, including transient wave propagation, liquefaction, landsliding, and surface fault rupture. Most historical ruptures of buried pipelines during earthquakes have occurred as a result of co-seismic ground failure and not the transient passage of the seismic waves themselves. Accordingly, the management of seismic hazards and the implementation of risk reduction measures should be based mainly on risk-based assessments of co-seismic geohazards. This paper describes state-of-practice methodologies for both screening-level pseudo-probabilistic and system-wide fully probabilistic co-seismic geohazard risk analysis. The first step involves inventorying pipeline crossings of potentially active faults and terrain with susceptibility to co-seismic liquefaction and landslides. A logic-tree approach is then employed to incorporate epistemic uncertainty in geotechnical parameters along a pipeline system. Pseudo-probabilistic approaches involve applying seismic displacement prediction models to estimate either displacement at a target exceedance-probability level or frequency of exceeding a displacement threshold. Fully probabilistic approaches integrate seismic hazard curves and displacement prediction models to develop displacement hazard curves at each co-seismic geohazard crossing. These curves are combined with fragility models, obtained from empirical data or finite-element analyses, to estimate annualized rupture frequency at each crossing, which may be summed to estimate total system co-seismic rupture frequency.

Keywords: Place any keywords here

NOMENCLATURE

λ	annual rate of exceedance
AEP	annual exceedance probability
a_c	critical acceleration
D	displacement
DHC	displacement hazard curve
DV	decision variable
EDP	engineering demand parameter
IM	intensity measure
k_y	yield acceleration
L	loading parameter
M	magnitude
PGA	peak ground acceleration
PGD	permanent ground displacement
PGV	peak ground velocity
PSHA	probabilistic seismic hazard analysis
R	distance to the source
S	site parameters
SDPM	seismic displacement prediction model
TGD	transient ground displacement
T_s	fundamental period
UHRS	uniform hazard response spectra
V_s	shear wave velocity
w	weight

1. INTRODUCTION

This paper outlines a methodology for the development of seismic displacement hazard curves (DHCs) at pipeline

Comentado [AB1]: update

Comentado [YA2R1]: updated

crossings of terrain with credible potential for co-seismic ground failure, as a requisite input into pipeline risk analyses. The general approach involves:

- identifying locations with susceptibility to co-seismic ground failure
- performing seismic hazard analysis to obtain hazard curves and disaggregations of the hazard by magnitude and tectonic region type
- developing representative soil shear strength models that incorporate logic trees to capture a range of credible shear-strength values and groundwater levels for mapped geological deposit type
- performing screening-level analysis using semi-empirical and empirical seismic displacement prediction models (SDPM) for landsliding and triggering analysis for liquefaction
- Developing DHCs by integrating seismic hazard curves and SDPMs for liquefaction and lateral spreading that incorporate relative contributions of crustal and subduction earthquakes

The work described herein is part of a system-wide seismic hazard analysis for a pipeline corridor in western Canada. It will be combined with site-specific fragility curves developed using finite element modelling, to incorporate local variation in burial depth, pipeline orientation with respect to ground movement, length of pipe embedded in moving ground, and other site-specific mechanical and geometric considerations. This paper is limited to the SDPM component of the scope; subsequent work will integrate fragility models to develop total annual pipeline failure probability estimates and prioritize crossings on a risk basis for seismic risk reduction efforts. Probabilistic and pseudo-probabilistic approaches to estimating co-seismic ground failure hazard are described.

2. BACKGROUND

2.1. Pipeline Vulnerability to Seismic and Co-Seismic Hazards

Buried pipelines may experience loss of serviceability or loss of product containment during earthquakes as a direct result of transient stress changes arising from seismic wave propagation or the indirect effects of co-seismic permanent ground displacement (PGD) due to fault displacement, liquefaction, or landsliding (O'Rourke and Liu, 1999; Lanzano et al. 2014; Nyman and Bouckovalas 2019; Figure 1). Temporary displacement of soil caused by the propagation of seismic waves is referred to as transient ground deformation (TGD); the damaging effects of TGD are generally proportional to the Peak Ground Velocity (PGV) of the passing seismic waves (Lanzano et al., 2015). Ground surface displacement caused by surface faulting, liquefaction, or earthquake triggered landslides is referred to as permanent ground deformation (PGD). Co-seismic liquefaction and landslides triggering is generally proportional to the peak ground acceleration (PGA). Lanzano et al. (2015) determined that PGD has accounted for more pipeline incidents than TGD based on case-history data from global earthquakes.

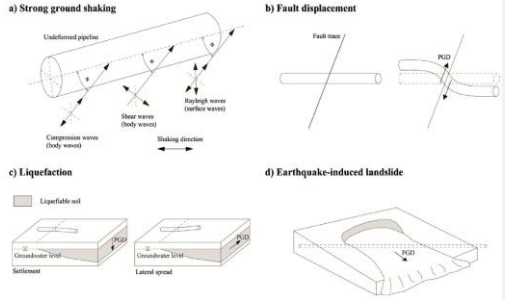

FIGURE 1: PIPELINE FAILURE MECHANISMS IN EARTHQUAKES. FROM LANZANO ET AL. (2014).

Surface fault rupture typically occurs along or near geological faults with documented historical and/or prehistorical activity (Baize et al., 2020). Surface fault rupture hazard is therefore higher in active tectonic areas and where Quaternary faults are present.

Liquefaction may occur where loose, saturated soils are subjected to strong earthquake shaking, causing a sudden increase in pore-water pressure, decrease in effective stress, and loss of shear strength. Liquefaction probability increases with PGA and is possible in susceptible soils where PGA exceeds 0.09 g (Santucci de Magistris et al., 2013). PGD caused by liquefaction has been observed in M > 4.5 earthquakes (Ambraseys, 1988; Green and Bommer, 2018). Pipeline integrity impacts are rare where liquefaction manifests as settlement or sand boils, but more common in lateral spreads and flows triggered by liquefaction (Honegger et al., 2006). Liquefaction susceptibility is related to geologic age and depositional environment (e.g., Youd and Perkins, 1978; Quinn et al., 2015). Honegger and Nyman (2017) recommend that the design of most pipeline projects consider liquefaction where they cross sedimentary deposits with high or very high liquefaction susceptibility, as per the Youd and Perkins (1978) qualitative classification system.

Co-seismic landslides can occur where PGA experienced in an earthquake exceeds a slope's critical acceleration (a_c), which is the horizontal acceleration required to reduce the factor of safety against sliding below unity. At a given location, screening-level a_c may be calculated using an infinite-slope pseudostatic limit-equilibrium model (Wieczorek et al., 1985; Wilson & Keefer, 1985). A magnitude threshold for PGD related to earthquake triggered landslides and surface faulting is approximately Mw 5.0 (Keefer, 1984; Rodriguez et al., 1999; Baize et al., 2020).

2.2. Project Context and Description

The subject of the work was a pipeline corridor through the Canadian Cordillera, connecting producing regions in the

Western Canadian Sedimentary Basin with a marine export terminal in southwestern British Columbia. Seismic hazard is relatively high along the southwestern portion of the study region, owing to its proximity to the Cascadia Subduction Zone. The forearc region, west of the Coast Mountains, is subject to periodic megathrust earthquakes with magnitudes up to about 9, frequent intraslab earthquakes deep below ground surface within the down-going Juan de Fuca plate, and strong earthquakes on crustal faults in the overriding Pacific Plate where oblique subduction causes forearc compression and deformation (Figure 2). Seismic hazard is moderate through the Rocky Mountains but low through the central Cordillera and in the Plains east of the Cordillera.

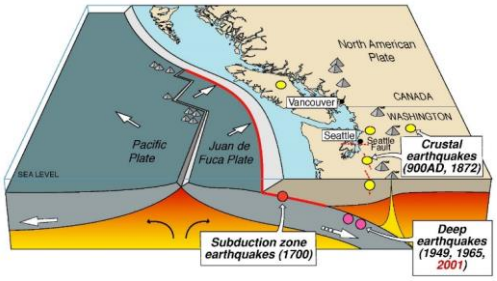

FIGURE 2: CASCADIA SUBDUCTION ZONE SEISMOTECTONIC SETTING. IMAGE SOURCE: USGS.

The pipeline owner's objectives were to (1) estimate the annual system-wide risk of pipeline rupture or facility damage due to seismicity and co-seismic processes, and (2) identify locations that contributed most to the total system-wide annual hazard, such that they could be prioritized for risk reduction measures. The work builds upon earlier efforts to map terrain susceptible to co-seismic ground failure and develop earthquake monitoring and response systems.

The project benefitted from extensive subsurface geotechnical information, including approximately 1700 boreholes; and project-specific terrain maps that classified geological deposit types and geomorphic processes. Available borehole data included SPT blow counts, shear vanes, Atterberg limits, and grain size distributions. Boreholes were more densely spaced at crossings of watercourses, roads, railroads, and known areas of slope instability, and otherwise relatively sparse.

3. OVERVIEW OF PROCEDURES

The following workflow was implemented for co-seismic landslide hazard sites:

1) Inventory potential hazard sites.
2) Calculate the seismic resistance of the slope (i.e., critical acceleration, a_c)
3) Perform probabilistic seismic hazard analyses
4) Perform a screening-level assessment using a pseudo-probabilistic approach at 1/2475 annual exceedance probability (AEP)
5) Develop displacement hazard curves for site with non-negligible displacement determined in the screening-level assessment
6) Perform pipe-soil interaction analysis to develop pipeline strain response curves.
7) Estimate probability of pipeline failure as a function of pipe strain.
8) Calculate the vulnerability of the pipeline at various seismic hazard return periods to develop a pipeline failure hazard curve.

The following workflow was implemented for lateral spreading hazard sites:

1) Inventory potential hazard sites.
2) Perform probabilistic seismic hazard analyses
3) Calculate probability of triggering liquefaction, screening sites where liquefaction triggering probability is negligible at 1/2475 AEP.
4) Develop lateral displacement hazard curves for sites passing the screening-level assessment.
5) Perform pipe-soil interaction analysis to develop pipeline strain response curves.
6) Estimate probability of pipeline failure as a function of pipe strain.
7) Calculate the vulnerability of the pipeline at various seismic hazard return periods.

Holocene fault crossings are absent along the pipeline corridor; accordingly, faulting was excluded from the work scope.

4. SEISMIC HAZARD INVENTORY

Regional scale hazard assessments typically involve applying a SDPM on a grid basis across a wide area; however, this is computationally intensive and introduces challenges with selecting a representative landslide or lateral spreading zone that could impact the linear infrastructure. In this study, sites with potential for co-seismic landslides or lateral spreading hazards were first inventoried along the full pipeline corridor to limit detailed further analyses to crossings with non-negligible pipeline failure probabilities.

To delineate hazard sites associated with potential co-seismic landslides, critical accelerations were estimated using methodology developed by Wieczoriek et al. (1985) and Wilson and Keefer (1984). This methodology uses a simple shear strength model, in which mapped geological units are classified into three general groups, each of which is assigned an assumed friction angle and cohesion intercept. Project-specific terrain maps and published bedrock geological maps were the basis for geologic group assignments. Critical acceleration was calculated using an infinite-slope model, assumed slip-surface depth of 3 m, and assumed wet conditions (i.e., groundwater height at 2.4 m above the slip surface), and slope angle derived from a 25 m resolution digital elevation model. Potential co-seismic landslide sites were included in an inventory where calculated critical acceleration was generally less than 0.15 g and the slope angle

exceeded 8°. Approximately 300 landslide sites were inventoried using this process.

The inventory of lateral spreading sites was based on a liquefaction susceptibility classification system by Quinn et al. (2015) and Youd & Perkins (1978). Lateral spreading hazard sites were inventoried where the qualitative susceptibility rating was equal to or greater than 'high' (when using Quin et al. [2015]) or "moderate to high" (when using Youd & Perkins [1978]), and within 250 m of a free face or on ground steeper than 0.5°. Approximately 170 lateral spreading sites were inventoried using this process.

5. SCREENING-LEVEL ASSESSMENTS

To further focus the study, a screening-level pseudo-probabilistic assessment was performed. For co-seismic landslide hazard sites, the screening-level assessment involved calculating median displacement magnitudes at a 1/2475 AEP hazard level. A probabilistic seismic hazard assessment (PSHA) was performed at each site to obtain uniform hazard response spectra (UHRS) and disaggregation of the seismic hazard. SDPMs were implemented for crustal and subduction tectonic regions using Bray and Macedo (2019) and Macedo et al. (2023). A key input into the SDPM is a_c (also known as yield acceleration [k_y]).

5.1. Automated Stability Modelling

The typical approach for calculating a_c on a site-specific basis is to use a limit equilibrium slope stability model (e.g., Slope/W or Slide) which satisfies three equilibrium equations: moments, forces in the vertical direction, and forces in the horizontal direction. However, limitations arise when having to perform hundreds of slope stability runs over a range of material types, slope angles, and water table levels. When performing seismic slope stability modelling on a regional scale, an infinite-slope limit equilibrium model is typically used given the simplicity of the calculation (e.g., Wieczorek et al., 1985; FEMA, 2023). However, this model is generally applicable only to slopes composed of homogenous cohesionless soil, where the slip surface is shallow and parallel to the slope face (Duncan et. al., 2014). Limitations also arise when having to estimate the fundamental period of the landsliding mass (T_s) and for selecting a representative slope which could impact the pipeline. Given these limitations, a more robust stability model was desired. As such, BGC used an open-source python program called Pyslope[1] which performs limit equilibrium stability modelling based on the simplified Bishop procedure. Modifications were made to the python code to accommodate undrained shear strength ratios and application of a horizontal seismic load (k_h). Helper python scripts were developed to automate setting the soil parameters, slope height and angle, water table, and calculation of a_c.

[1] https://github.com/JesseBonanno/PySlope

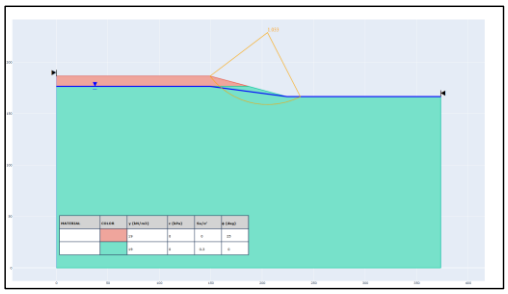

FIGURE 3: Example output of a stability model for a fine-grained material type.

To capture epistemic uncertainty in the soil strength models and groundwater levels used in the stability modelling, a logic tree approach was implemented (Ojomo et al., 2024; Figure 4). For each site and associated landslide slope, up to twelve a_c values were calculated. Undrained shear strength parameters were used for fine grained soil deposits and drained strength parameters were for coarse grained soil deposits.

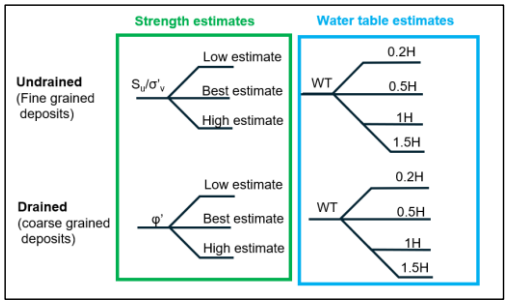

FIGURE 4: Logic tree approach for calculating a_c. H is equal to the height of the slope and water table depth (WT) was measured relative to the crest of the slope.

Soil strength parameters were correlated to project-specific terrain mapped surficial material types using available borehole data. Available borehole data included SPT blow counts, shear vanes, Atterberg limits, and grain size distributions, with approximately 1700 boreholes available.

Weightings were applied to each calculated a_c based on a log-normal distribution by calculating the mean and standard deviation of calculated a_c values associated with each site and landslide slope.

An additional output from stability modelling included calculating the initial fundamental period of the sliding mass (T_s) as recommended by Bray and Macedo (2019).

Comentado [AB3]: I changed this reference to be the closure doc.

Comentado [YA4R3]: added

$$Ts = \frac{4H}{V_s}$$

5.2. Pseudo-Probabilistic Displacement Modelling for Landslides

Using Bray and Macedo (2019b) and Macedo et al. (2023) as a SDPM and the inputs from the stability modelling, displacements were calculated for each site at a 1/2475 AEP seismic hazard level. Spectral accelerations (SA) were obtained at degraded fundamental periods of $1.3T_s$ from the total UHRS. Mean magnitudes for each tectonic region type (crustal and subduction) were obtained from disaggregations of the 1/2475 hazard level ground motions and used to calculate tectonic region-specific displacement magnitudes. The scalar model was used for crustal tectonic region types while the vector model (based on two intensity measure types) was used where peak ground velocity (PGV) exceeded 40 cm/s for interface earthquakes and 20 cm/s for intraslab earthquakes (Macedo et al., 2023). The total displacement associated with the median displacement prediction was calculated using a weighted average approach, where the percent contribution to the total hazard for each tectonic region type was used as a weighting factor. The displacements associated with each realization of the stability model logic tree (Figure 4) were then aggregated using the weightings of each a_c to provide a total displacement magnitude for each site. Any sites with less than a 5 cm median displacement magnitude threshold were removed from subsequent fragility analysis (Figure 5).

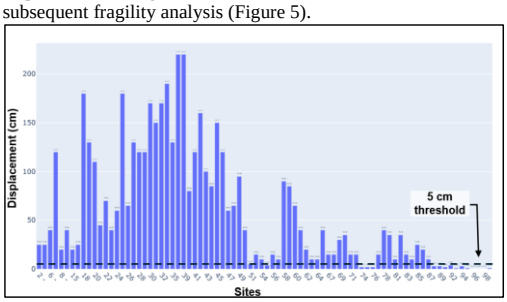

FIGURE 5: Bar chart example of pseudo-probabilistic displacement results for a subset of inventoried sites.

5.3. Liquefaction Triggering Analysis

For the screening-level analysis of lateral spreading sites, probability of triggering liquefaction was calculated using Idriss and Boulanger (2012) where borehole data were available, and using Federal Emergency Management Agency (FEMA) 2024 criteria for sites without available borehole data. The seismic hazard level used in the screening-level analysis was PGA at 1/2475 AEP, similar to the co-seismic landslide sites. In general, sites with a probability of triggering liquefaction greater than 0.05 were included for further analysis (e.g., development of displacement hazard curves and pipeline fragility).

6. PROBABILISTIC DISPLACEMENT ANALYSIS

Probabilistic hazard curves for lateral spreading and landslide displacement are grounded on the PEER performance-based framework (Deierlein et al., 2003), defined by:

$$\lambda(DV) = \iiint G\langle DV|DM\rangle dG\langle DM|EDP\rangle dG\langle EDP|IM\rangle d\lambda(IM)$$

Where λ(DV) is the mean annual rate of exceedance of a decision variable (DV), DM is a damage measure, EDP is an engineering demand parameter, IM is an intensity measure, and the terms in the equation are conditional probabilities independent of one another.

To obtain displacement hazard curves, where displacement is the EDP, additional conditional probabilities should be considered to include the conditional disaggregation of the ground motion hazard and rate of occurrence.

The seismic hazard underpinning the lateral spreading and landslide displacement analysis can be computed using the OpenQuake engine and the seismic models proposed by GEM. This tool provides hazard curves and disaggregation data, classified by tectonic region (crustal and subduction: interface and intraslab).

6.1. Landslide displacement hazard curves

The procedure to estimate probabilistic landslide displacement hazard curves (DHC) consists of solving this equation (Bray and Macedo, 2023):

$$\lambda(D > d) = \iint \lambda(IM) \cdot P\left(D > d \middle| IM, M, k_y, T_s\right) \cdot P(M|IM)\Delta\lambda(IM)d(IM)d(M)$$

Where λ(D>d) is the annual rate of exceedance of a threshold displacement *d*, M is magnitude, k_y is the yield acceleration, T_s is the initial fundamental period, and IM in this case can represent the spectral acceleration at a degraded period $1.3T_s$ (Sa(1.3Ts)) or peak ground velocity (PGV).

1) Each site's response spectrum is interpolated to estimate Sa(1.3Ts)) values at selected return periods.
2) Then, conditional probabilities of slope displacement, $P(D > d|IM)$, are computed per return period using the disaggregated M and tectonic region-specific ground motion levels with Bray and Macedo (2019) for crustal earthquakes and Macedo et al. (2023) for subduction earthquakes.
3) For each return period, the conditional probabilities are weighted by the disaggregation contributions and by the weights (w_{k_y}) assigned to k_y in the logic tree, to calculate $\sum P\left(D > d|IM, M, k_y, T_s\right) \cdot P(M|IM) \cdot w_{k_y}$
4) For each tectonic region, the rate of occurrence, $\Delta\lambda(IM)d(IM)$, is calculated to obtain DHC for each source type and IM. When the SDPM is dependent on two intensity measure types (i.e., vector model), the joint rate of occurrence is required. Macedo et al. (2023) provided a correlation coefficient for calculating the joint rate of occurrence.

5) In the last stage, the DHC are calculated by aggregating the DHCs for each tectonic region within each displacement bin.

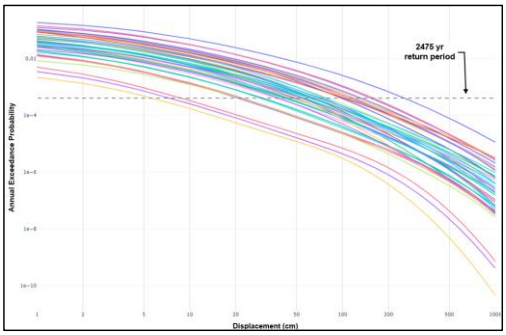

FIGURE 6: Example of a series of DHCs associated with co-seismic landslide hazard sites.

6.2. Lateral spreading displacement hazard curves

Youd et al. (2002) proposed a lateral displacement prediction equation that can be separated into two parts. One is the loading parameter (L) which is dependent on magnitude (M) and source-to-site distance (R) and the other is a site parameter (S) dependent on site specific conditions (e.g., $N_{1(60)}$, thickness of liquefiable unit, grain size, free-face height, and/or slope gradient, etc.), and ε represents uncertainty:

$$\overline{\log D_H} = L - S + \varepsilon$$

The loading part (L) of the Youd et al. (2002) equation can be used as an IM:

$$L = b_1 M + b_2 \log R^* + b_3 R$$

Where b_1, b_2, and b_3 are regression coefficients and R* is a distance parameter for near-source earthquakes

Franke and Kramer (2013) proposed a probabilistic framework for lateral spreading, solving this equation:

$$\lambda_{D_H}(d|S) = \sum \lambda(M|m) \sum \sum P(D_H > d|S, M = m, R = r) \cdot P(M = m, R = r)$$

Where $\lambda(M|m)$ is the mean annual rate of exceeding a minimum magnitude of interest for a given seismic source.

1) L is calculated from the disaggregated M, R values using a lognormal standard deviation.
2) Computed L values are used to generate exceedance probabilities across a range of thresholds (i.e., P(L>l)) using the cumulative distribution function.
3) Following the PEER framework, the joint probability distribution of L is calculated by weighting M and R by disaggregation contributions.
4) L values are translated into expected displacements with the site parameters. When borehole data was available at a site, site parameters were calculated for each borehole and a weight was assigned (generally an average). When borehole data was unavailable, three-point distribution of site parameters for each liquefaction susceptibility rating was applied and weighted according to a normal distribution.
5) Resulting displacement estimates were aggregated based on weightings for each site to produce a single displacement hazard curve.

7. RESULTS AND DISCUSSION

The approach described herein will yield seismic displacement hazard curves at each co-seismic landsliding and lateral spreading hazard crossing that meets the 1/2475 AEP screening threshold: median displacement exceeding 5 cm for landslides, and liquefaction probability exceeding 5% for lateral spreading sites. Once seismic displacement hazard curves are established for these sites, the next step would be to incorporate a vulnerability assessment. This could be performed at each site using screening-level criteria (e.g., Lanzano et al., 2015), but given the complexity arising for variable geometry at each crossing (e.g., burial depths, orientation of the pipeline with respect to the expected ground movement direction, length of pipe embedded in moving ground), a more appropriate approach would be to develop fragility curves on a site-by-site basis using finite-element modelling. At this time, the development of fragility curves remains in progress and will be the subject of future work.

The methodology described herein makes several simplifying assumptions. First, the geology of co-seismic geohazard sites is generally assumed to be uniform. Second, shear-strength values are assumed to be consistent within mapped geological units, in which logic trees capture epistemic uncertainty in shear-strength values. Accordingly, each unit is represented by a range of potential shear-strength values, rather than a single value based on observed conditions (i.e., from boreholes and geotechnical testing at every location). Third, conservative site-classes were used when performing PSHAs. Fourth, the approach uses simplified limit-equilibrium models with simplified stratigraphy, and semi-empirical and empirical seismic displacement prediction models. It is expected that pipeline rupture probability might be inaccurate on a site-by-site basis, but that the aggregated risk across the pipeline system should be relatively representative. As such, locations that are identified as having an elevated likelihood of experiencing large ground displacements, or, after the next stage of developing fragility models, would have an elevated probability of failure, would be best assessed by reducing uncertainty in the input shear strength model through site-specific geotechnical studies, and/or replacing empirical DPMs with site-specific displacement analysis.

8. CONCLUSION

The approach described in this paper represents a first step in analyzing system-wide seismic risk. It describes the geotechnical hazard analysis component: specifically, the development of seismic displacement hazard curves for pipeline

crossings. Subsequent work will integrate vulnerability models to enable a system-wide risk analysis.

ACKNOWLEDGEMENTS

The project benefitted from reviews by Saman Zarnani of BGC Engineering and Dr. Jorge Macedo of Georgia Tech University.

REFERENCES

[1] O'Rourke, M.J., Liu, X., (1999). Response of Buried Pipelines Subjected to Earthquake Effects, MCEER Monograph, 3. University of New York at Buffalo, US.

[2] Lanzano G, Salzano, E., Santucci de Magistris, F., & Fabbrocino, G. (2014). Seismic vulnerability of gas and liquid buried pipelines. *Journal of Loss Prevention in the Process Industries*, *28*, 72-78. http://dx.doi.org/10.1016/j.jlp.2013.03.010

[3] Nyman, D., & Bouckovalas, G. (2019). Assessment and Mitigation of Seismic Geohazards for Pipelines. In Rizkalla, M., & Read, R.S. (Eds.), *Pipeline Geohazards: Planning, Design, Construction and Operations*. ASME Press.

[4] Lanzano, G., Santucci de Magistris, F., Fabbrocino, G., Salzano, E. (2015). Seismic damage to pipelines in the framework of Na-Tech risk assessment. *J. Loss Prev. Process Ind. 33*, 159–172.

[5] Baize, S., Nurminen, F., Sarmiento, A., Dawson, T., Takao, M., Scotti, O., Azuma, T., Boncio, P., Champenois, J., Cinti, F.R., Civico, R., Costa, C., Guerrieri, L., Etienne, M., McCalpin, J., Koji, O., & Villamor, P. (2020). A Worldwide and Unified Database of Surface Ruptures (SURE) for Fault Displacement Hazard Analysis. *Seismological Research Letters. 91*(1), 499-520.

[6] Santucci de Magistris, F., Lanzano, G., Forte, G., Fabbrocino, G. (2013). A database for PGA threshold in liquefaction occurrence. Soil Dynamics and Earthquake Engineering, 54: 17-19.

[7] Ambraseys, N. (1988). Engineering Seismology. Earthquake Engineering and Structural Dynamics, 17, 1, 1-50.

[8] Green, R.A., Bommer, J.J. (2019). What is the smallest earthquake magnitude that needs to be considered in assessing liquefaction hazard? Earthquake Spectra 35: 1441-1464.

[9] Honegger, D.G., Nyman, D.J., Youd, T.L. (2006). Liquefaction hazard mitigation for oil and gas pipelines. Eight U.S. National Conference on Earthquake Engineering, San Francisco, CA, April 2006.

[10] Youd, T.L. and Perkins, D.M. (1978). Mapping of liquefaction induced ground failure potential. Journal of Geotechnical Engineering Division, v.104, no. GT4, American Society of Civil Engineers, Reston, VA, p.433-446.

[11] Quinn, P., Zaleski, M., Mayfield, R., Karimian, H., Waddington, B. (2015). Liquefaction susceptibility mapping derived from terrain mapping; experience on a linear project in British Columbia, Canada. GeoQuebec.

[12] Honegger, D., Nyman, D. (2017) Pipeline seismic design and assessment guideline. Technical report, Pipeline Research Council International, Inc., Virginia.

[13] Wieczorek, G.F., Wilson, R.C., and Harp, E.L. (1985) Map showing slope stability during earthquakes in San Mateo County California: U.S. Geological Survey Miscellaneous Investigations Map I-1257-E, scale 1:62,500.

[14] Wilson, R.C., and Keefer, D.K. (1985) Predicting areal limits of earthquake-induced landsliding, in Ziony, J.I., ed., Evaluating Earthquake Hazards in the Los Angeles Region—An Earth-Science Perspective: U.S. Geological Survey Professional Paper 1360, p. 316-345.

[15] Keefer, D.K., 1984, Landslides caused by earthquakes: Geological Society of America Bulletin, v. 95, p. 406-421.

[16] Rodriguez, C.E., Bommer, J.J., Chandler, R.J. (1999). Earthquake-induced landslides: 1980-1997. Soil Dynamics and Earthquake Engineering, 18 (5), 325-346.

[17] Bray, J.D., and Macedo, J. (2019). Closure to Procedure for Estimating Shear-Induced Seismic Slope Displacement for Shallow Crustal Earthquakes by Jonathan D. Bray and Jorge Macedo. Journal of Geotechnical and Geoenvironmental Engineering, ASCE, V. 145(12).

[18] Bray JD, Macedo J. (2019b) Procedure for estimating shear-induced seismic slope displacement for shallow crustal earthquakes. J Geotech Geoenviron Eng 2019;145. (12):04019106.

[19] Macedo J, Bray JD, Liu C. (2023) Seismic slope displacement procedure for interface and intraslab subduction zone earthquakes. J Geotechnical Engineering.

[20] Duncan, J., Wright, S., and Brandon, T. (2014) Soil strength and slope stability. 2nd Ed, John Wiley and Sons, Inc., Hoboken.

[21] Boulanger, R. W., and Idriss, I. M. (2012) Probabilistic SPT-based liquefaction triggering procedure. J. Geotech. Geoenviron. Eng., 1185–1195.

[22] Deierlein, G.G., Krawinkler, H., and Cornell, C.A. (2003). A framework for performance-based earthquake engineering. 2203 Pacific Conference on Earthquake Engineering.

[23] Bray, J.D. and Macedo, J. (2023). Performance-based seismic assessment of slope systems. Soil Dynamics and Earthquake Engineering, 168, 107835.

[24] Youd, T. L., Hansen, C. M., and Bartlett, S. F. (2002) Revised multilinear regression equations for prediction of lateral spread displacement. J. Geotech. Geoenviron. Eng., 128 (12), 1007–1017.

[25] Franke, K.W. and Kramer, S.L. (2013). Procedure for the empirical evaluation of lateral spread displacement hazard curves. J. Geotech. Geoenviron. Eng. 140 (1), 110-120.